EOLIAN SAND TRANSPORT MONITORED BY TERRESTRIAL LASER SCANNING

R. Lindenbergh [a,*], S. Soudarissanane [a], S. de Vries [b], M. Coquet [b], M. de Schipper [b], K. Hejbudzka [a], K. Duijnmayer [a], B. van Goor [a] and A. Cohen [c]

[a] Dept. of Remote Sensing, Fact. of Aerospace Eng., Delft UT, Kluyverweg 1, 2629 HS, – (r.c.lindenbergh, s.s.soudarissanane, k.a.hejbudzka)@tudelft.nl, koen.duijnmayer@gmail.com, b.vangoor@student.tudelft.nl
[b] Dept. of Hydraulic Eng., Fact. of Civil Eng. and Geosciences, Delft UT, Stevinweg 1, 2628 CN, – (Sierd.deVries, M.A.deSchipper)@tudelft.nl, marion-coquet@hotmail.fr
[c] Deltares, Stieltjesweg 2, 2628 CK – Anna.Cohen@deltares.nl

Delft, The Netherlands

Commission VI, WG VI/4

KEY WORDS: Terrestrial laser scanning, Change detection, Eolian transport, Coastal monitoring

ABSTRACT:

Morphodynamic changes at sandy coasts, as are dominant in The Netherlands, are typically monitored at yearly intervals by means of LIDAR. Meanwhile it is recognized that beach morphodynamics is not a regular process but is strongly correlated to meteorological conditions. A time series of 14 terrestrial laser scans of a beach experiment is analyzed, obtained during a time period of 88 hours characterized by changing weather conditions including strong wind and rain. It is shown that after a conversion to a suited spherical grid, different deformation regimes can be identified and that elevation changes rates below a millimeter an hour can be detected.

1. INTRODUCTION

In the Netherlands, the most densely populated areas are situated directly behind the coastal defense and partly below the mean sea level. The Holland coast is approximately 124 km long and consists mainly of sandy beaches protected by a dune system (Short, 1991). The sandy coastal system protects the hinterland while providing an important natural and recreational zone. Unfortunately it is renowned to suffer from structural erosion. It is therefore vital to understand the physical system of the sandy Dutch coast at high level to mitigate ongoing erosion and upcoming sea level rise. Current national coastal policy is to maintain the coastline position seaward of its 1990 position. This is achieved by applying a total amount of approximately 15×10^6 m^3 of sand per year in nourishments on the beach and shoreface. How this nourished sand is redistributed over the surrounding coast in time remains a question.

The coastline position and associated beaches are monitored at yearly intervals by the Ministry of Transport, Public Works and Water Management (JARKUS measurements). Since the year 2000, measurements of the beach until the first dune row are obtained by airborne laser scanning. Based on these measurements and on similar foreshore bathymetric surveys, it is decided where, when and how the coastal system should be supported by beach or shoreface nourishments. Although these regular airborne laser scanning surveys provide valuable information on the state of the coast, it is also recognized that morphodynamic changes in the coastal system are in general not at all regular. High energy events, such as storms, typically result in instantaneous large changes. Apart from storm events, the beach topography is constantly changing at a scale depending on e.g. wind speed, wind direction and sand fetch.

To further investigate the scale of the morphodynamic changes affecting the beach topography, an experiment was designed to measure sand transport. The experiment took place at a sandy beach about 15 km south of the city of The Hague in The Netherlands, at a location called Vlugtenburg. At the beach, at about 100 m from the high water line, a screen of about 10 m long and 1 m high was built up. The screen consisted of a plastic sheet maintained with wooden polls deeply stabilized in the sand. As the wind blew from slightly different directions, the screen was not put completely straight. It was approximately oriented perpendicular to the wind direction. At about 10m in the direction of the wind, an extra high tripod was solidly set-up deep in the sand. From the tripod the topography was sampled by the terrestrial laser scanner Faro Photon 120 during a period of 88 hours. In total 73 scans were captured during 15 epochs, ranging between November 2 2009, 5 PM and November 6 2009, 9 AM.

During this period of 88 hours, wind, mainly from the SW direction was prominent and many showers occurred. Although the scanner was removed from the tripod between epochs, a small wooden roof protecting the scanner during measurements turned out to be quite useful. Additionally, wooden targets were scattered in the scene to enable registration of the different scans. As these targets positions were also measured using GPS, the resulting point clouds could be transformed in a global coordinate system. At each epoch, three to four scans were acquired in a row to compensate for possible problems in individual scans, due to for example strong rain or sudden wind gusts. During the

* Corresponding Author

Figure 1: Experiment setup: sand particles transported towards the plastic screen and the wooden house protecting the terrestrial laser scanner Faro Photon 120.

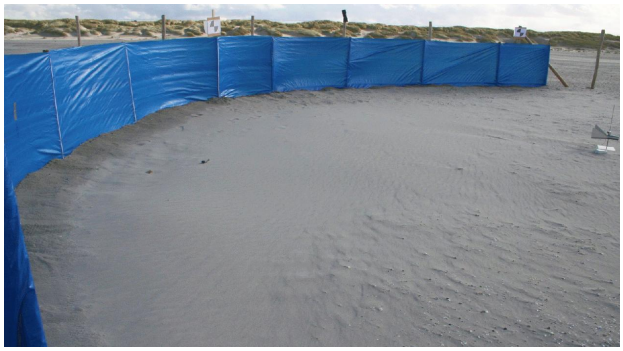

Figure 2: Sand screen, checkerboard targets and saltiphone; Accumulation of sand in front of the screen is visible as well.

experiment, several meteorological parameters were monitored, which were mainly considering the wind, while the amount of sand blowing over the beach was quantified using so-called saltiphones, (Spaan and Van den Abeele, 1991).

In this paper, an initial analysis of a suited selection of one scan per epoch will be described. After the registration of all selected scans in a common coordinate system, non-terrain points are removed from each scan. The remaining points in each scan are sampled to a spherical grid, adaptive to the distance to the scanner in such a way that each grid point value is estimated by approximately the same amount of scan points. Sampling each scan to the same grid enables a time series analysis per grid point. Fitting a linear time trend to each of the approximately 50000 grid points reveals several deformation regimes that will be discussed in the results section.

Based on the initial analysis presented here, it will be decided how the available scans should be processed in order to obtain optimal conclusions on the topographic changes that occurred at the beach part during monitoring. Elsewhere it will be reported how these morphodynamic changes link to wind parameters and sand transport rates as measured by the saltiphones.

2. BEACH EXPERIMENT DATA

In this section, the topographic data obtained for the beach experiment is described. An overview of the experiment is shown in Figures 1 and 2. In both figures, the screen is clearly visible and is facing the wind. The expectation on forehand was that sand is transported by wind, provided the wind is strong enough. Near the screen, the wind force will drop, and as a consequence, the sand in the air will be deposited. To optimally profit from the screen, it is important that its orientation is perpendicular to the wind direction. Therefore it was decided at one instance during the experiment to adjust the screen position: at one side it was shortened, while meanwhile it was extended at the other side. The final aim of the experiment is to link the sand volume changes in front of the screen to the meteorological and saltiphone data. The volume changes will be determined based on the terrestrial laser scans.

Between epochs, the scanner had to be removed from the tripod, because of the bad weather conditions and to prevent theft. As a consequence neither it can be assumed that each scan was obtained from the same location nor that the scanner was oriented in the same direction. Therefore it was necessary to align all scans obtained in a common coordinate system in a registration procedure. For this purpose, paper targets mounted on small wooden boards were used, as weakly visible in Figures 1 and 2.

2.1 GPS measurements

The location of the targets has been measured by GPS, to enable an accurate alignment in (finally) the Dutch coordinate system RDNAP. Coordinates of the target have been obtained by both real time kinematic measurements and by post-processed static measurements. In all cases, the reported standard deviations are in the order of 1 cm in horizontal position and in the order of 1.5 cm in the vertical. The targets have been measured by GPS at the end of the measurement campaign, at around hour 70. Because of the bad weather conditions, it is quite likely that the position of some of the targets has moved by a few centimeters during the measurement campaign.

2.2 Terrestrial laser scans

In total 73 scans were obtained using the FARO Photon 120 terrestrial laser scanner. On forehand it was expected that the effective range on the beach would be about 20 m: given a scanning height of 2m on a flat beach, the angle between the incoming laser range and the up surface normal amounts to 85 degrees. This means that at larger distances both the point density and point quality will deteriorate. The expectation on the effective scan distance came approximately true in practice. As stated in the introduction some redundant scans were obtained to avoid loss of information. Although winds from the South to WestSouthWest occurred with a force of up to 6 Beaufort, accompanied by daily precipitation rates between 5-10 mm, no loss of scan data was observed. For this first analysis it is chosen to consider a set of 14 scans, specified in Table 1:

Scan ID	Scan time	Scan hour	Millions of points	M. points filtered
006	N2 16:52	0	21.2	6.1
012	N2 22:09	5	22.1	6.8
016	N3 07:50	15	22.5	6.5
020	N3 09:02	16	21.7	6.2
025	N3 13:44	21	21.6	6.1
032	N3 22:05	29	21.6	6.8
038	N3 23:42	31	21.6	6.7
042	N4 08:25	39	21.8	6.6
046	N4 12:36	44	21.7	6.7
050	N4 16:53	48	22.3	6.7
055	N4 21:55	53	21.5	6.2
060	N5 11:09	66	21.9	6.5
079	N5 17:46	73	33.8	9.6
086	N6 09:13	88	34.4	9.1

Table 1: Overview of processed scans. In the second column, N2 stands for November 2, 2009. Hours are in GMT +1.

3. PROCESSING TIME SERIES OF SCANS

3.1 Registration

Using the visibility of the paper targets in the Faro Scene software, all scans in Table 1 were registered based on these control points. Additionally all scans were converted to the RDNAP coordinate system by applying the GPS coordinates. The final accuracy achieved after registration and geo-referencing is better than 5 cm. The approximate position of the laser scanner in RD is estimated at (x,y) = (68824.025,447138.770). To facilitate processing and presenting, the first two, resp. three digits of the x-, resp. y-coordinate will be discarded in the following, that is the approximate position of the scanner will be considered to be (x,y) = (824.025,138.770). In practice, the referencing of terrestrial laser scans for applications with a critical signal to noise ratio is in some sense an iterative procedure: initial referencing results should be carefully evaluated and if necessary improved. In the topic covered here, the signal to noise ratio is critical, and almost the complete scanned scene is subject to little movement (transport of sand).

Moreover, the targets used for referencing were not all stable due to heavy weather conditions. Therefore the initial results should be interpreted with care.

3.2 Extracting terrain points

Many scan points captured do not represent the beach topography, but are the results of reflections on notably i) the wooden construction protecting the scanner, and, ii), the screen as visible in Fig. 1, iii) targets, equipments and existing structures such as polls. First points clearly above the beach were removed by a hard threshold. Then only points fulfilling two criteria were kept, using an intermediate result of a segmentation algorithm described in Rabbani et al.(2006). For each scan point the 8 nearest neighbors were determined and a plane was fitted through these neighbors including the scan point itself. If the normal of this plane has an angle of less than 30 degrees with the up direction and if the standard deviation of the plane fit is below 2 mm, a point is considered to represent the terrain. In the last column of Table 1, the number of points for each scan remaining after this step is given. On average, only 30 % of the initial scan points remain after applying these filter steps.

3.3 Down sampling to adaptive spherical grid

In this experiment, only scans obtained from approximately the same scan position are compared through time. One method to compare such time series of scans is to sample or interpolate all scans to the same grid, (Lindenbergh and Hanssen, 2003; Lindenbergh, 2010). As in this case, the area of interest is approximately flat and horizontal; the point density strongly decreases with increasing distance to the scanner, as descibed in the following part. Let H denote the height of the scanner above the ground, and suppose the scanner scans with increasing vertical angle φ. The vertical angle, $\varphi_{Rk,}$ corresponding to a scan point at horizontal distance R_k is given by Eq. (1):

$$\varphi_{Rk} = \arctan(R_k / H). \quad (1)$$

If the scanner has a vertical angle increment of $\Delta\varphi$, the horizontal distance R_{k+1} to a scan point with a vertical angle $(\varphi_{Rk} + \Delta\varphi)$ is given by Eq. (2):

$$R_{k+1} = H \tan(\varphi_{Rk} + \Delta\varphi) - \tan \Delta\varphi. \quad (2)$$

Applying Eq. (2) allows defining a spherical grid centered at the position of the scanner such that each grid cell contains approximately the same amount of scan points. As an example, by considering a scanner height of H = 2.40m, and an angular increment of $\Delta\varphi$ = .25˚, the distance in the direction away from the scanner between grid points is about 1 cm at 1 m from the scanner, but more than half a meter at 20m from the scanner. For this paper a horizontal angular increment of 1˚, and a vertical angular increment of .25˚ is used for distances to the scanner between 1.13m to 30m. The horizontal angular increment determines the distance between grid points at equal horizontal distance of the scanner. The resulting grid consists of 107217 grid points. In practice, the number of grid points for each epoch is smaller, because not every grid cell contains scan points. An example of a point density adaptive spherical grid can be seen in Figures 3 and 4. The number of scan points per grid cell using these settings is in the order of 40 to 50.

For each grid cell, a height value of the grid point center is determined using inverse squared distance interpolation with power parameter $p = 2$, (El-Sheimy et al., 2002).

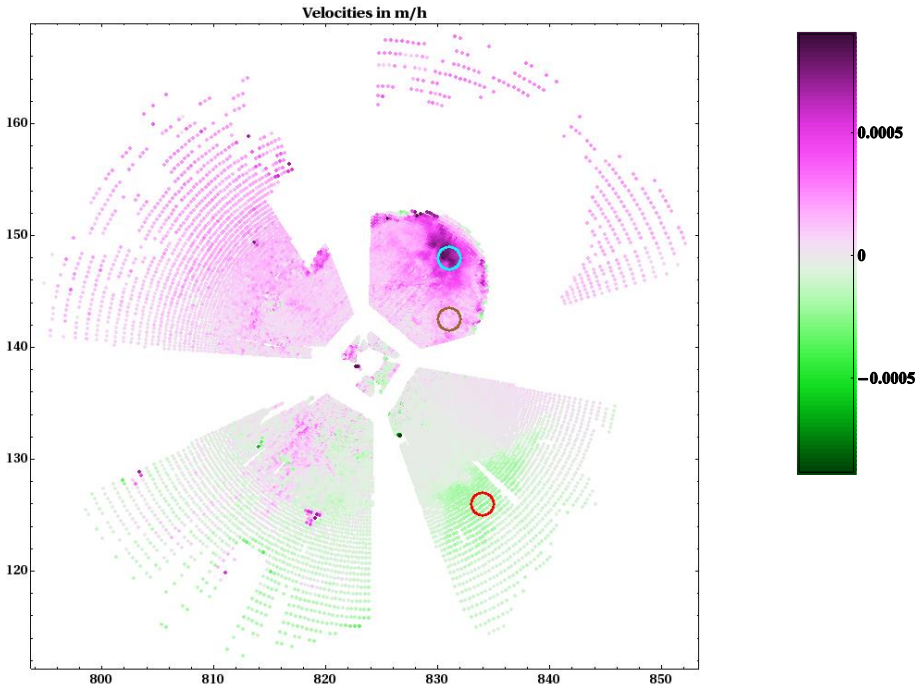

Figure 3. Mean sand erosion/accumulation in meter per hour. The cyan circle, at *(x,y) = (831,148)* corresponds to an area characterized by sand accumulation. Near the brown circle, *(x,y) = (831,142.5)*, the terrain is almost stable, while at the red circle, *(x,y) = (834,126)*, a small erosion trend was found. The trends at the grid points near the three circles are visualized in Figure 5.

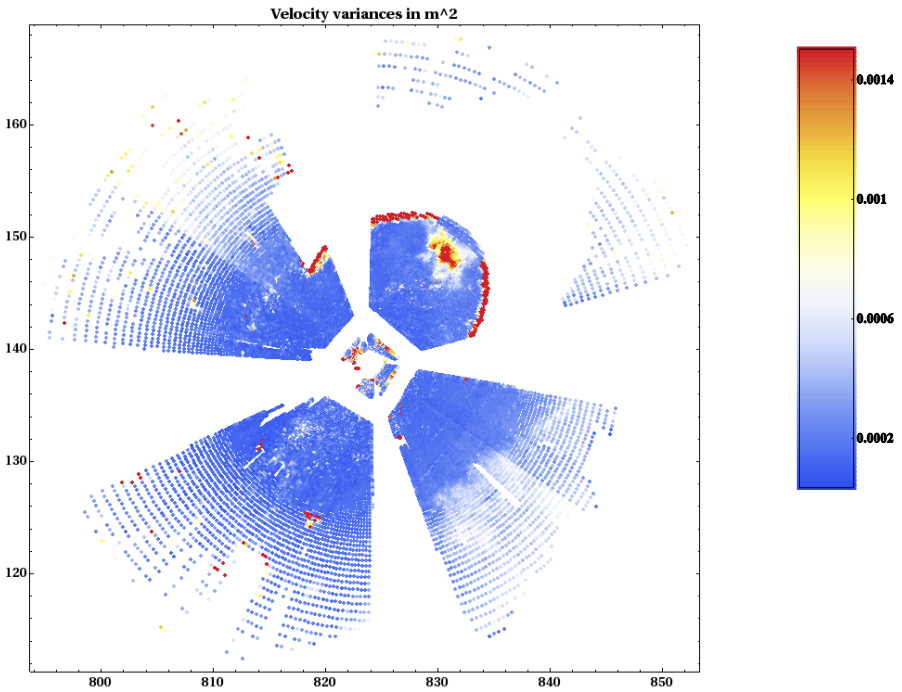

Figure 4. Variance of the estimated erosion/deposition trends.

3.4 Time series analysis

As a result of the previous step, 14 spherical grids are obtained, one for each scan as listed in Table 1. In the following only those grid cells are considered, for which a grid cell height was found in each of those 14 epochs. To obtain insight in possible erosion/deposition patterns, a time linear trend is estimated through each time series of grid cell heights. As there is no clear reason why possible erosion/deposition rates should be constant in time, it is also important to consider simultaneously the quality of fit of the rates found. Based on the initial results of such linear trend analysis, a division into locally coherent deformation regimes can be made. Other larger deviations can be recognized i) close to the position of the scanner, and ii) near the edges of

the available grid points. In both cases these deviations are believed to correspond to (small) non-terrain objects that were not or not completely removed by the filtering procedure.

4. DEFORMATION RESULTS

In this section a first analysis of the different erosion/deposition patterns is presented, as identified by the grid point analysis.

4.1 Available grid points

In Figures 3 and 4 the resulting spherical grid, adaptive to the horizontal distance to the scanner, is shown. Only those grid points are plotted for which a height value is present for each of the 14 epochs of Table 1, after the cleaning steps described in Section 3,. Several features can be recognized in the figures. The small white circle, near location *(x,y) = (824.025,138.770)*, corresponds to the location of the scanner. Around this circle a rectangular structure of missing grid points can be seen, with further fans of missing grid points starting at each of the corners of the rectangle. These points are all caused by the wooden structure protecting the scanner that is visible in Figure 1. Either points were reflected on the structure itself and where therefore removed as non-terrain points, or points on the terrain could not be scanned, because they were located in the scan shadow of the structure.

In the upper right part of the figure, many grid points are missing as well. These are mainly points on the terrain in the shadow of the screen, compare Figures 1 and 2. Besides, locally other grid points are missing due to the presence of for example beach poles or tools from the measurement team.

4.2 Local erosion/deposition trend results

In Figure 3, a local erosion/deposition rate in meter per hour is given for each grid point for which height values could be obtained in all 14 scans covering the total period of 88 hours, compare Table 1. It should be noted that relatively large rates are still only in the order of less than 1 mm per hour. Clearly an area in front of the screen, near location *(x,y) = (831,148)* can be recognized where a relatively large accumulation trend is detected. This is the effect that was expected while designing the experiment: because of the screen, the wind velocity will drop, resulting in sand deposition.

In fact, results are most clear when considering Figures 3 and 4 simultaneously. In Figure 4, the quality of fit of the linear time trends of Figure 3 are presented as a variance value. Large deviations from a linear fit are detected for the same are in front of the screen. Therefore we will consider these trends in more detail below. In addition, large deviations are also found directly at the left and right base of the screen. The reason for these deviations is the fact that the screen has been moved at one occasion, because of a change in wind direction. This also explains why no large deviations are visible in the middle of the base of the screen: that part was not changed during the experiment.

4.3 Different deformation regimes

In Figure 5, the actual time series of grid point elevations are shown for the three areas highlighted in Figure 3 by a circle. For each of the three plots in Figure 5, the twenty grid points closest to the circle centers in Figure 5 are selected. The colors are random. When comparing the three plots, some jumps in elevation are common to all three plots, notably the jump of almost 2 cm after 46 hours. It should be further investigated if those jumps are caused by problems with the registration.

The top plot in Figure 5 corresponds to the area in front of the screen where relatively large sand deposition trends were found. From the figure it is clear why the quality of linear fit is low (compare Figure 4). After a quiet start, elevation increases strongly between hours 17 and 45, after which the elevation stabilizes again. This regime can be directly linked to the weather conditions as experienced by the measurement team. In the middle plot in Figure 5, time series of elevations corresponding to the more stable area near location *(x,y) = (831, 148)* are shown. What should be noted here is that between hours 17 and 45 the elevations show a relative large variation. A possible explanation is that the bad weather conditions during this period caused some movement in either the targets or the scanner. In the bottom plot a small negative elevation trend can be observed, again most strong and rough during the bad weather period between hours 17 and 45. In Figure 3, a larger green patch is visible around *(x,y) = (834,126)* where apparently some sand loss took place. A morphodynamic explanation for this local sand loss cannot yet be given at this moment.

4.4 Further steps

Based on the results presented here, it will be first considered if the registration of scans of individual epochs can be improved, starting with those epochs where jumps are observed in the times series in Figure 5. In a next step, terrain change rates between epochs will be converted into sand volume changes. As the area of each grid cell is known, this step is reasonably straightforward. Except for a most likely volume change, also an error estimate of this volume change will be estimated, based on a formal error propagation of notably scan quality and registration quality. These results, purely based on the terrestrial laser scans, will then in detail be compared and linked to the meteorological observations and eolian sand transport rates as derived from the saltiphones.

5.CONCLUSIONS

In this paper we have discussed a first analysis of 14 beach scans obtained from the same position within a period of 88 hours. The scans of each of the 14 epochs were reduced to a spherical grid adaptive to the distance to the scanner. A trend analysis per grid point revealed different deformation regimes allowing the identification of elevation change rates of less than a millimeter an hour. The initial results presented here demonstrate that a terrestrial laser scanner can be successfully used to identify local morphodynamic changes at the millimeter level even during harsh weather conditions consisting of strong rain and wind.

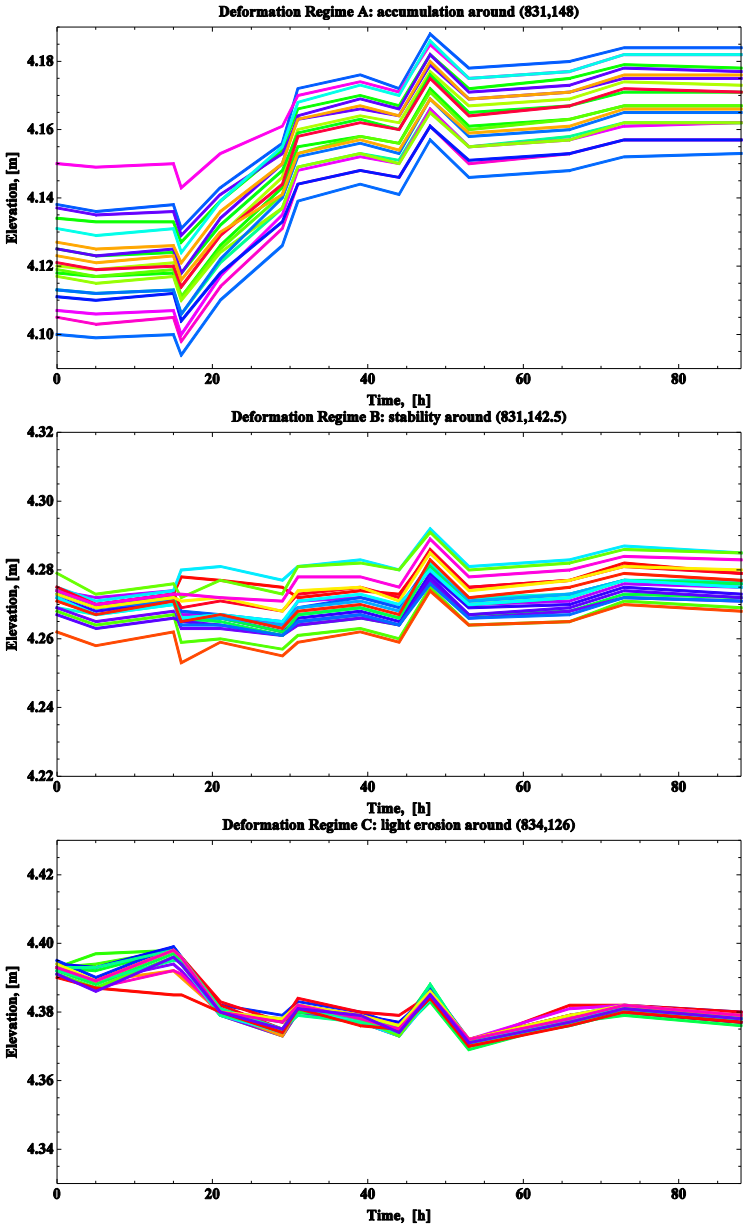

Figure 5: Three different deformation regimes. In each figure, time series are shown for the 20 grid points closest to the location indicated in the figure label, compare also the three circles in Figure 3.

6. ACKNOWLEDGEMENTS

The work presented here is part of the Building with Nature project, Work package `Hollandse Kust` 3.2, Monitoring dune compensation Delfland. Roderik Koenders is thanked for help with the Word software.

7. REFERENCES

El-Sheimy, N., Valeo, C. and Habib A., 2005. *Digital Terrain Modeling - Acquisition, Manipulation and Applications*, Artech House.

Lindenbergh R.C., 2010. Book Chapter: Engineering Applications, In *Airborne and Terrestrial Laser Scanning*, G. Vosselman and H.-G. Maas (Eds.), Whittles Publishing.

Lindenbergh, R.C. and Hanssen, R., 2003. Eolian deformation detection and modeling using airborne laser altimetry. In: *Proceedings IGARSS 2003*, Toulouse, France.

Rabbani, T., Van den Heuvel F.A. and Vosselman G., Segmentation of point clouds using smoothness constraint, *IAPRS* **36**(5) (2006), pp. 248–253.

Short, A.D., 1992. Beach systems of the central Netherlands coast: Processes, morphology and structural impacts in a storm driven multi-bar system. *Journal of Marine Geology*, 107(1-2),
pp. 103-137.

Spaan, W. and Van den Abeele, G.D., 1991. Wind borne particle measurements with acoustic sensors. *Soil Technology* 4(1), pp. 51–63.